

Possible applications of bubble acoustics in Nature

T. G. Leighton, P. R. White and D. C. Finfer

*Institute of Sound and Vibration Research, University of Southampton, Highfield,
Southampton SO17 1BJ, UK*

Gas bubbles are the most potent naturally-occurring entities that influence the acoustic environment in liquids. Upon entrainment under breaking waves, waterfalls, or rainfall over water, each bubble undergoes small amplitude decaying pulsations with a natural frequency that varies approximately inversely with the bubble radius, giving rise to the 'plink' of a dripping tap or the roar of a cataract. When they occur in their millions per cubic metre in the top few metres of the ocean, bubbles can dominate the underwater sound field. Similarly, when driven by an incident sound field, bubbles exhibit a strong pulsation resonance. This paper discusses three examples of how bubble acoustics may find applications in Nature. The first of these is the determination of bubble size distributions through inversion of the sound fields that bubbles generate on entrainment. This can be used not only in testing models of bubble cloud evolution under breaking waves, but also in extraterrestrial environmental assessment. The second application lies in the possible enhancement by humpback whales of the efficiency of the bubble nets they use in fishing. The third speculates on the apparent conundrum, that unless dolphins employ better signal processing than humans currently do, then when they hunt in bubble-rich environments (such as might be found near the sea surface or in bubble nets) they are, in these visually confusing environments, nullifying their own most spectacular sensory apparatus.

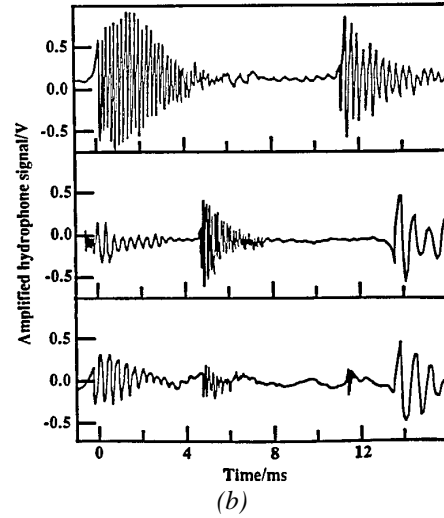
1. INTRODUCTION

The study of bubble acoustics contains a wealth of fascinating physics [1,2]. The ideal spherical pulsating bubble acts as a damped oscillator: the stiffness comes from the bubble gas (which exerts a restoring force when the bubble volume changes); and the inertia is invested primarily in the surrounding liquid, which is set into motion when the bubble wall moves. Viscous, thermal and acoustic radiation losses contribute to the damping.

As linear oscillators at low amplitudes of pulsation, gas bubbles in liquids are abundant, and responsible for many of the sounds we associate with liquids in the natural world. Section 2 explores examples of what can be learned when such sounds are interpreted in terms of the bubble population which created them. When driven by external sound fields, a bubble exhibits a powerful pulsation resonance (plus potentially numerous resonances associated with higher order spherical harmonic shape perturbations, although with some exceptions [3-5] these make negligible contribution to the far field emissions). The influence of that pulsation resonance on the sound speed underwater, and on acoustic attenuation and scatter, is explored in this paper through speculation as to the roles they may play in cetacean acoustics (section 3).



(a)



(b)

Figure 1. (a) Three selections from the hydrophone sound recording made at the site shown in part (b). The recordings contain characteristic exponentially decaying sinusoids, each of which indicates the bubble source is a lightly damped oscillator, the radius of which can be determined from the natural frequency. Here the counting of bubbles is made simple because the low entrainment rate means there is little overlap between bubble signatures. (b) One author (TGL, age 21) at Kinder Scout in the Peak District (Derbyshire, UK), taking the recording shown in (a). After Leighton and Walton [8].

2. INVERTING BUBBLE ENTRAINMENT EMISSIONS TO ESTIMATE BUBBLE POPULATIONS

After entrainment by breaking waves, waterfalls, injectors etc., the lightly-damped bubble pulsation emits, into the far field, an approximately exponentially decaying sinusoidal acoustic pressure signature at the natural frequency (Figure 1). Although bubbles are capable of undertaking the complete range of oscillations which the orders of spherical harmonic perturbation can describe, with some exceptions [5-7] it is the pulsation mode (zero order) which, as a monopole, contributes most effectively to the sound which propagates away from the bubble. The first measurements [8] of the size distribution of bubble population in the natural world using these ringing emissions were made in 1985. The technique of inferring bubble radii in the natural world from the natural frequencies they emit (Figure 1), has given rise to hundreds of studies [9], from rainfall sensing [10,11] to industrial sparging [1,12-19] (the injection of gas under pressure through a liquid in order to facilitate processing). Development of this technique included use of the Gabor Transform [11,20] and spectral methods for when entrainment rates are high [1,9]. A tutorial on such acoustic inversions is available via the web [21].

Such techniques are based on the known relationship between the radius of a bubble and its natural frequency. The passive emissions and resonances from bubbles appear to be ubiquitous because entrainment on Earth (by injection, pouring, wave breaking *etc.*) typically generates bubbles having radii ranging from millimetres to microns. These provide pulsation natural frequencies in the frequency range of at least ~1-500 kHz respectively (with commensurate quality factors of roughly 30 to 5). This radius-to-frequency mapping follows from a small-amplitude expansion of the nonlinear equation of motion [1] for the pulsations of a bubble about an equilibrium radius R_0 . In the long

wavelength limit ($kR_0 \ll 1$, where k is the acoustic wavenumber), the resulting damped circular natural frequency ω_b is:

$$\omega_b = \frac{1}{R_0 \sqrt{\rho_0}} \sqrt{3\kappa \left(p_0 - p_v + \frac{2\sigma}{R_0} \right) - \frac{2\sigma}{R_0} + p_v - \frac{4\eta^2}{\rho_0 R_0^2}} \quad , \quad (1)$$

where p_0 is the static pressure in the liquid outside the bubble, η and ρ_0 are, respectively, the shear viscosity and mass density of the liquid (which is assumed to be incompressible), p_v is the vapour pressure, σ is the surface tension, and κ is the so-called polytropic index. This engineering term is not a fundamental quantity, but takes an intermediate value between γ (the ratio of the specific heat of the gas at constant pressure to that at constant volume) and unity, depending on whether the gas is behaving adiabatically, isothermally, or in some intermediate manner (such that the ideal gas relationship between the bubble volume (V) and its gas pressure (p_g) can vary between $p_g V^\gamma = \text{constant}$ and $p_g V^1 = \text{constant}$). Note that the use of a polytropic law only adjusts the way gas pressure changes in response to volume changes to account for heat flow between the gas and its surroundings. In most bubble acoustics models where it is used, κ takes a constant value over the oscillatory cycle and, used in this way, can never describe net thermal damping during the oscillatory cycle of a bubble [22]. However the polytropic index does adjust the bubble stiffness for this heat flow.

In fact equation (1) only includes damping due to shear viscosity η , which has the expected effect for a linear oscillator, such that the damped natural frequency is lower than the undamped one (obtained by setting $\eta = 0$). Equation (1) does not incorporate thermal or acoustic radiation losses, which require more sophisticated models [1]. Other corrections may be required to account for bubble-bubble interactions [23,24], and models of the behaviour of bubble clouds show that these can possess natural frequencies much lower than those of the individual bubbles which make up the cloud [25,26].

The assumption of free field conditions underpins the vast majority of the theory of bubble acoustics, including equation (1). However almost all of the experimental realisations of bubble acoustics are not in the free field, and neglect of this can lead to errors in damping [27] of $\sim 100\%$. Usually there is some acoustically free surface present (such as an atmosphere/liquid interface), which will generate reverberation. In addition, important classes of bubble oscillation also occur in tubes [28-31] (including ear canals and blood vessels) [32,33], in pipes [34], and in a variety of other geometries. Indeed, the generation of conical [35-38] bubbles led to spectral studies [39] and applications in needle-free biomedical injectors [40].

A simplified form of (1) was first derived by Minnaert [41] in 1933. He assumed adiabatic conditions ($\kappa = \gamma$) and no damping ($\eta = 0$). He also neglected the effects of vapour pressure and surface tension (i.e. $p_v = 0$ and $\sigma = 0$, respectively). In this limit equation (1)

takes a particularly simple form, such that the undamped natural frequency ω_0 is inversely proportional to the equilibrium bubble radius R_0 . For air bubbles in water under Earth surface conditions, this holds true for roughly $R_0 > \sim 15 \mu\text{m}$, such that $\omega_0 R_0 / 2\pi \approx 3 \text{ Hz m}$. This means that the O(mm) bubbles entrained in brooks and streams produce an audio-frequency babble, whereas an O(MHz) biomedical sound field might excite the resonance of a micron-sized bubble.



Figure 2. The Salmon Leap, Sadler's Mill, Romsey (Longitude $1^{\circ}30'$ W; Latitude $50^{\circ} 59'$ N). (a) Side view, looking to the West-South-West. (b) View to the South-South-West, looking downstream towards the Broadlands estate. The hydrophone was placed at a depth of 10 cm in clear water, about 3 m from the turbulent bubble cloud. (Photographs: T G Leighton).

An interesting study was undertaken to show the extent to which we might invert the acoustic signal emitted by entrained bubbles to obtain information on the bubble population, and to demonstrate how useful this might be. The sound of the waterfall at Sadler's Mill, Romsey, UK (Figure 2(a),(b)) was recorded, and its spectrum is shown by the blue line in Figure 3. This spectrum was then used in an inversion calculation [42] to estimate the size distribution of 'ringing' bubbles. This required an appropriate model for the emission from each bubble. Reference [1] details the model [1,9] used for the inversion, with the amplitude determined by the surface tension, the bubble size, and the depth at which it is entrained [42].

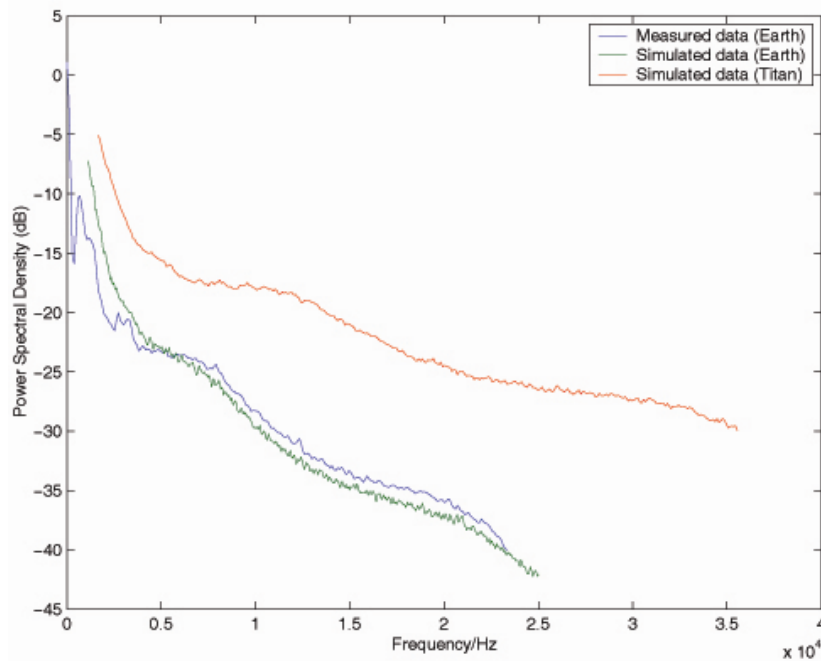
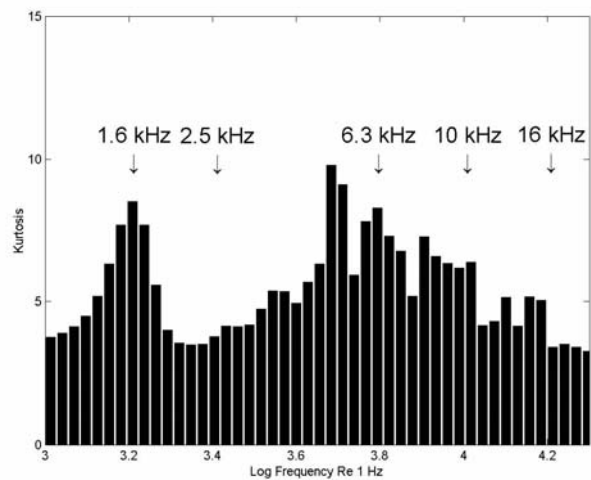


Figure 3. Power spectral densities of 10 s signals. Blue line: The signal recorded at site of Figure 2, from which those components due to bubbles were identified and used to infer the population of bubbles. Green line: The predicted signal for Earth from the bubble population obtained by inverting the data of the blue line. Red line: The signal predicted for the same bubble population, were it to be entrained on Titan. After reference [42].



Figure 4. An artist's impression of Titan's surface, with Saturn dimly in the background through Titan's thick atmosphere. The *Cassini* spacecraft flies over the surface with its High Gain Antenna

pointed at the Huygens probe as it nears the end of its parachute descent. Thin methane clouds dot the horizon, and a narrow methane spring or "methanefall" flows from the cliff at left and produces considerable vapour. Smooth ice features rise out of the methane/ethane lake, and crater walls can be seen far in the distance. (Illustration by David Seal, Image credit: NASA/JPL/Caltech).



(a)

Order	Moment and/or statistic	Fourier transform of moment
2	Variance	Power spectrum
3	Skewness	Bispectrum
4	Kurtosis	Trispectrum

(b)

Figure 5. (a) The kurtosis of the Earth waterfall data of the blue line of Figure 3. Note that the kurtosis tends to be greater than 3, and therefore is super-Gaussian. (b) Classification of statistics and moments of signals.

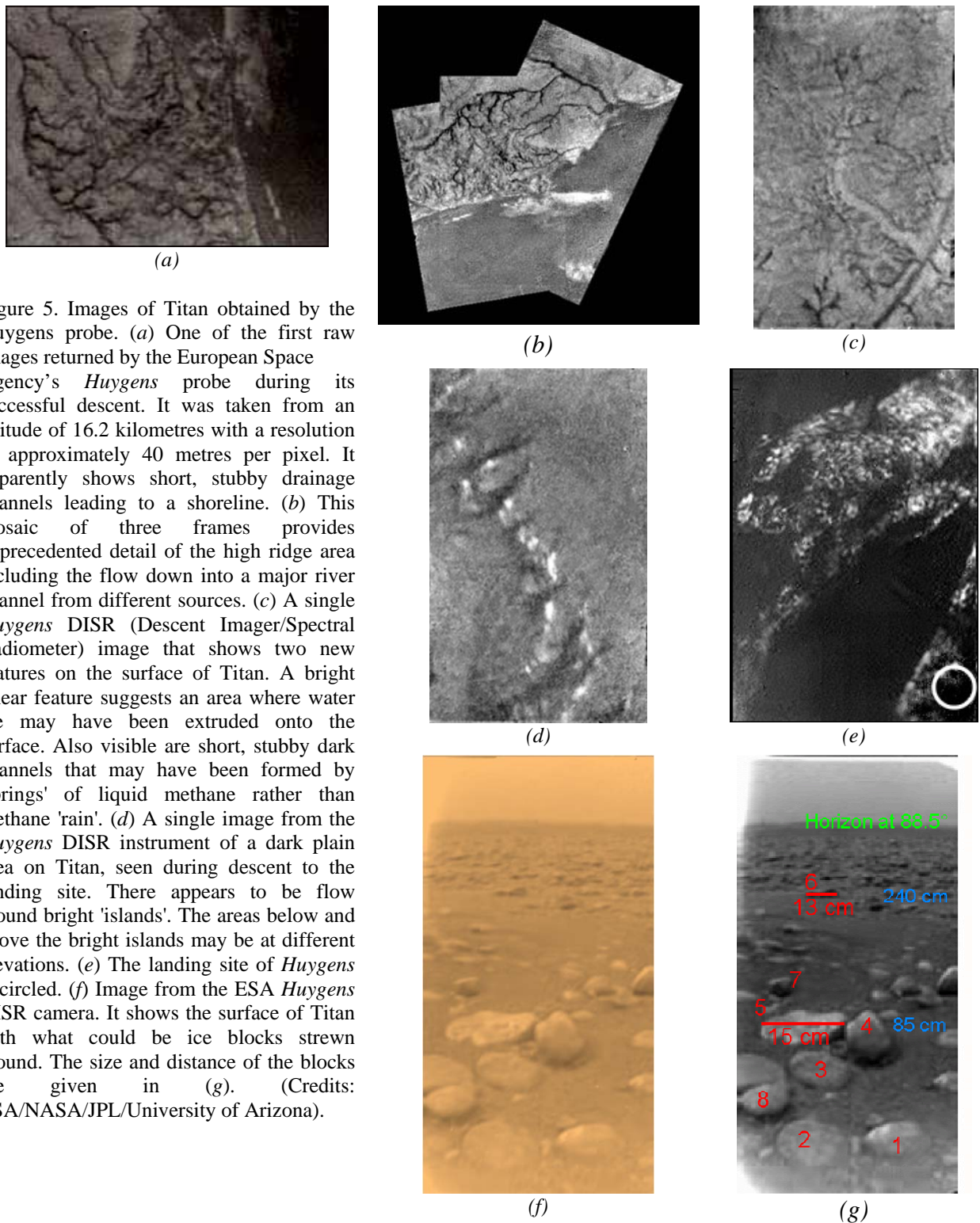


Figure 5. Images of Titan obtained by the Huygens probe. (a) One of the first raw images returned by the European Space Agency's *Huygens* probe during its successful descent. It was taken from an altitude of 16.2 kilometres with a resolution of approximately 40 metres per pixel. It apparently shows short, stubby drainage channels leading to a shoreline. (b) This mosaic of three frames provides unprecedented detail of the high ridge area including the flow down into a major river channel from different sources. (c) A single *Huygens* DISR (Descent Imager/Spectral Radiometer) image that shows two new features on the surface of Titan. A bright linear feature suggests an area where water ice may have been extruded onto the surface. Also visible are short, stubby dark channels that may have been formed by 'springs' of liquid methane rather than methane 'rain'. (d) A single image from the *Huygens* DISR instrument of a dark plain area on Titan, seen during descent to the landing site. There appears to be flow around bright 'islands'. The areas below and above the bright islands may be at different elevations. (e) The landing site of *Huygens* is circled. (f) Image from the ESA *Huygens* DISR camera. It shows the surface of Titan with what could be ice blocks strewn around. The size and distance of the blocks are given in (g). (Credits: ESA/NASA/JPL/University of Arizona).

Having obtained an estimate of the population of 'ringing' bubbles, this population was then entered as input into the model, with appropriate parameters for Earth, in an attempt to reconstruct the sound of the Sadler's Mill waterfall artificially (Figure 3, green line). Having therefore some confidence in the technique (based on the similarity of these two

spectra), it was supposed that there is a methane-fall on Titan (the largest moon of Saturn) which entrains the same bubble size distribution as was found at Sadler's Mill (Figure 4). As the BBC reported in 2004, 'According to Professor Leighton, "If there is a splash and not a crunch when the probe lands, that would make Titan the first known body other than Earth to have an ocean open to an atmosphere. This would mean there could be babbling brooks and streams; and a beach at minus 180 degrees C"'.

It was decided that if this is the case, then first the sound of a splashdown should be predicted, to determine to what extent it would be recognisable. This was done, and the results can be found via the web site [21]. Then by using the Sadler's Mill population as input into the model, and using physical parameters appropriate for Titan, it was possible to predict the spectrum of the resulting sound (Figure 3, red line) [42]. Recordings of these sounds, and similar predictions of possible splashdown sounds, can be accessed via the web page [21]. Work is continuing in analysing the higher moments of these signals to provide a more taxing test than simply through matching the spectra (second order moment) as was done in Figure 3 (see Figure 5).

In fact, during its descent on January 14 2005 (one week prior to the presentation on which this paper is based), *Huygens* photographed features which are currently believed to reflect the presence of flowing liquid on Titan, which carves out valleys and presumably is likely to generate methane falls (Figure 6(a)-(d)). The landing site, though possibly close to such an area (Figure 6(e)), is thought to be on a mud- or snow-like surface (Figure 6(f),(g)), and hence the microphone on the probe did not detect the sound of either a splashdown or a methane fall.

The purpose of this exercise is to demonstrate the opportunities which acoustic measurements offer for space exploration. The signal has low bandwidth, the hardware is rugged, and typically has low mass, low cost, and low power requirements. Given the myriad uses for diagnosis by bubble-generated sound on Earth, from rainfall sensing to investigating atmosphere/ocean mass flux, this exercise illustrates that the use of sound in general as an extraterrestrial diagnostic presents intriguing possibilities.

One example of the powerful new ways in which acoustics has been used in oceanographic problems like this, is illustrated in Figure 7. It should be noted [1,2,22] that the bubble populations measured by the passive techniques described above, differ from the populations measured by the active acoustic techniques, which transmit an applied acoustic field into a region of bubbly water and infer the bubble size distribution present from the bubble-mediated changes to sound speed, attenuation or scattering. Passive emissions come only from those bubbles which are actively 'ringing'. This emission occurs only within the first few milliseconds after entrainment for most bubbles. Inversion of passive acoustic emissions will therefore estimate the population size distribution of 'ringing' bubbles. Optical and active acoustic techniques actually measure the size distribution of a different bubble population, comprising not only the ringing bubbles but also the silent bubbles which have ceased to ring, but which nevertheless persist in the water column. By comparing the results of active and passive measurements, it is possible to test dynamic models for the evolution of bubble clouds and so investigate the processes which occur beneath a breaking wave (such as turbulence, circulation, buoyancy, etc. – Figure 7)

[22,43]. These processes convert the population initially produced by the breaking wave (the one measured by the passive acoustic technique) into the background population (as measured by the active acoustic technique). The resulting experiment [22,43] involved deployment of a range of acoustic sensors into the surf zone (Figure 8).

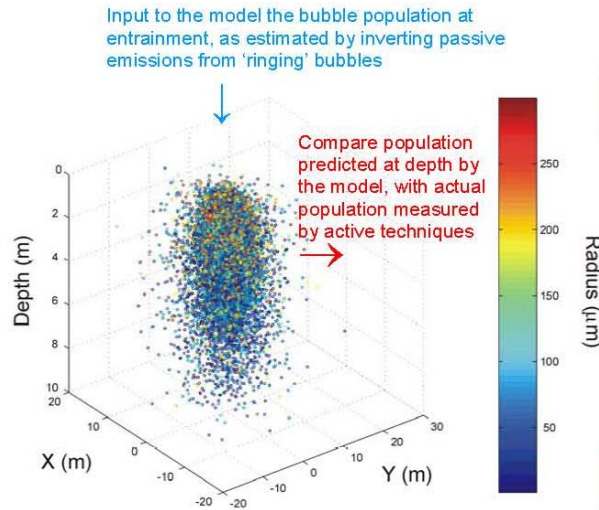


Figure 7. A single frame from an animation illustrating the evolution of an oceanic bubble cloud, following its entrainment beneath a breaking wave. The air/sea interface is flat and at depth 0 m. The plot shows a 3D section of ocean measuring 40 m x 50 m x 10 m deep. The ocean itself is infinitely deep (although alternative models including seabeds are available via the associated web page [21]). Into this section of ocean is injected a bubble population. This ‘ringing’ population is based on measurements of the passive noise from breaking waves. The bubbles are placed in a cube measuring 0.5 m on a side, the top side being in the centre of the horizontal air-sea interface region shown. The population then evolves under the influence of buoyancy, turbulence, surface tension and hydrostatic pressure, and gas flux occurs as for example the bubbles dissolve [44]. (One process not yet included in this model is bubble coalescence and fragmentation [11,20,45]). The frame shows the bubble cloud about 30 s after injection. The bubble size distribution is colour coded, and it is for example clear that whilst turbulence has dispersed the cloud spatially, both buoyancy and hydrostatic effects result in the tendency for small bubbles (blue) at depth, with the larger (yellow/orange/red) bubbles tending to occur only close to the surface. The accuracy of such models were investigated [43] by comparing the predicted bubble population as a function of depth with the measurements [22] of active acoustic techniques. Each of the 64000 bubbles in the simulation must represent approximately 10^4 bubbles in nature because of computational limitations. For further details see the associated web page [21].

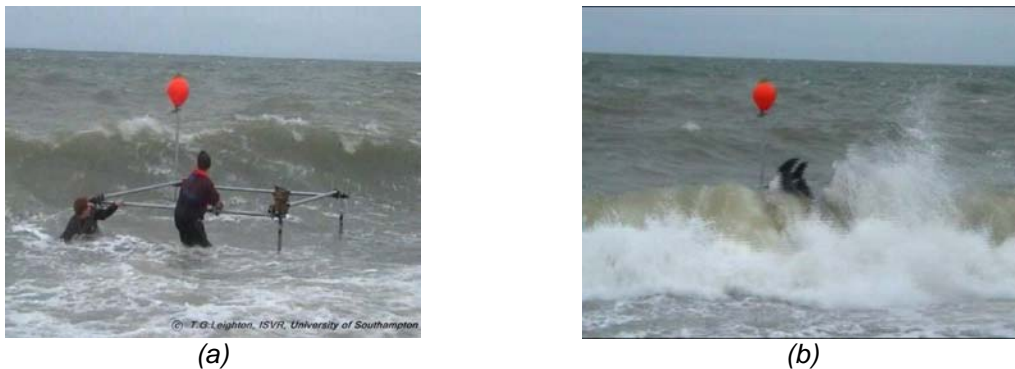


Figure 8. Two photographs, taken a fraction of a second apart, showing (a) two of the author’s students (S.D. Meers and M.D. Simpson) attempting to bolt sensors to a scaffolding rig the team have just deployed at sea; (b) Mr Simpson’s feet (Mr Meers is not visible). During the subsequent trial the winds increased from the calm conditions shown here to speeds in excess of 50 mph. Taken from Leighton *et al.* [22].

3 CETACEAN BUBBLE ACOUSTICS

Marine mammal calls often propagate through bubbly water, be it generated under breaking waves, in wakes, or even by the mammals themselves. Two circumstances are of particular interest: the possible use of acoustic signals to trap prey in bubble nets; and the ability of dolphin sonar to operate in bubbly water (such as the surf zone) that would confound the best man-made sonar, despite the fact that the dolphins possess ‘hardware’ which is comparatively mediocre [46].

3.1 The bubble nets of humpback whales

For many years there has been speculation as to the mechanism by which humpback whales (*Megaptera novaeangliae*) exploit bubble nets to catch fish [47]. It has been known for decades that single whales, or groups, might dive deep and then release bubbles to form the walls of a cylinder, the interior of which is relatively bubble-free (Figure 9(a),(b)) [48]. The prey are trapped within this cylinder, for reasons previously unknown, before the whales lunge feed on them from below (Figure 9(c)). There is evidence that prey can be contained by the bubbles alone. However it is certainly known that when a proportion (as yet unquantified) of humpback whales form such nets, they emit very loud, ‘trumpeting feeding calls’, the available recordings containing energy up to at least 4 kHz. Leighton *et al.* [47] proposed that these whales may be using such calls to enhance the ability of their bubble nets to trap the fish, in the following manner. A suitable void fraction profile would cause the wall to act as a waveguide. Assume the scales permit the use of ray representation. Figure 10 shows how, with a hypothetical tangential insonification, the mammals could generate a ‘wall of sound’ around the net, and a quiet region within it. The natural schooling response of fish to startling by the intense sound as they approach the walls would, in the bubble net, be transformed from a survival response into one that aids the predator in feeding [47]. The frequencies in the feeding call are indeed in the correct range to excite resonances in fish swim bladders and, given their sensitivities [49], presumably such excitation could discomfort the fish sufficiently for it to return to the interior of the net.

Figure 10(b) plots the raypaths (calculated using standard techniques [50]) from four whales whose beampatterns are represented by a 10° fan of 281 rays, for a bubble net in which the void fraction increases linearly from zero at the inner and outer walls, to 0.01% at the mid-line of the wall. The proposed ‘wall of sound’ and quiet interior are clearly visible. Even if the whales do not create sufficiently directional beams and insonify tangentially, the bubble net might still function through its acoustical effects. The ‘wall of sound’ effect in Figure 10(b) is generated from those rays which impact the wall at low grazing angles. Those rays which never impact the wall do not contribute to the ‘wall of sound’. If rays of higher grazing angle impact the net, they may cross into the net interior, though their amplitudes would be reduced by the bubble scattering, and attenuation alone would generate a quieter region in the centre of the net.

The actual acoustics of the cloud will of course be complicated by 3D effects and the possibility of collective oscillations; and even, speculatively, bubble-enhanced parametric

sonar effects [51] which might be utilized by whales, for example to reduce beamwidth or generate harmonics, sum- and difference-frequencies *etc.*.



(a)



(b)

Figure 9. (a) Schematic of a humpback whale creating a bubble net. A whale dives beneath a shoal of prey and slowly begins to spiral upwards, blowing bubbles as it does so, creating a hollow-cored cylindrical bubble net. The prey tend to congregate in the centre of the cylinder, which is relatively free of bubbles. Then the whale dives beneath the shoal, and swims up through the bubble net with its mouth open to consume the prey ('lunge feeding'). Groups of whales may do this co-operatively (Image courtesy of Cetacea.org). (b) Aerial view of a humpback bubble net (photograph by A. Brayton, reproduced from [52]).



(c)

(c) Humpback whales lunge feeding (Image courtesy of L. Walker, <http://www.groovedwhale.com>).

At frequencies sufficiently high to drive the bubble cloud in an inertia-controlled fashion, the bubbles produce an increase in sound speed. The wall is outwardly-refracting, and rays are no longer trapped within the cloud. The refractive effect of these bubbles on sound speed becomes negligible at even higher frequencies, although of course acoustic attenuation and scatter may be great. A variety of ray behaviours is possible, from reflecting straight off the net to traversing it and the interior with barely any refraction (Figure 10(c)) [47]. Such frequencies would not be effective in trapping prey, even if the prey could perceive them. However if scattering losses permit (and it is by no means certain they would), is it possible that, given these refracted paths, such frequencies could be used for echolocation of the contents of the net?

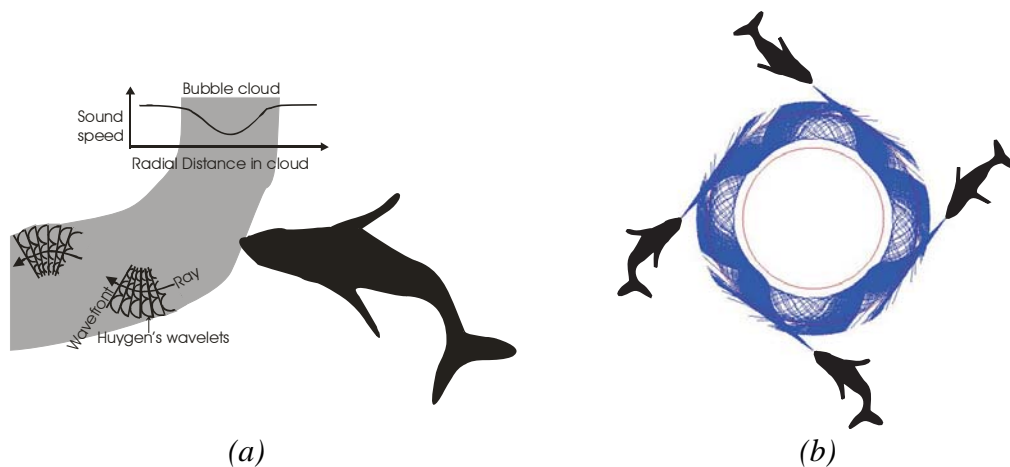
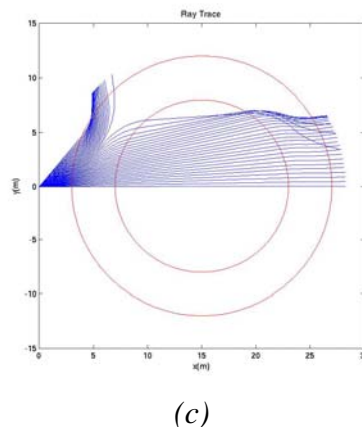


Figure 10. (a) Schematic of a whale insonifying a bubble net (plan view), illustrating the sound speed profile in the cloud and, by a Huygens construction, sample ray paths. The sound speed profile assumes void fractions are greatest in the mid-line of the net wall, and assumes that the bubbles pulsate in stiffness mode. Hence the closer a Huygens wavelet is to the mid-line, the smaller the radius of the semicircle it forward-plots in a given time. Rays tend to refract towards the mid-line. (b) Four whales insonify an annular bubble net described in the text. The inner red circle represents the inner boundary of the net wall (the outer boundary, also red, is obscured by rays). The ray paths are computed using 281 rays with an angular extent of



10° . These refract as in (a). The rays gradually leak out, although some rays can propagate around the entire circumference. Plotting of a raypath is terminated when it is in isovelocity water and on a straight-line course which will not intersect the cloud. This refers to rays whose launch angles are such that they never intersect the net; and to rays which, having entered the net and undertaken two or more traverses of the mid-line, leave it. (c) Example ray paths computed for the case where the sound speed increases towards the centre line of the annular bubble net. For this simulation, however, the source has a 45° beamwidth in order to illustrate the variety of ray bending that is possible (a 10° beam, as used in (b), tends to cause all rays follow a similar path, either traversing the net or refracting out of it, depending on the angle with which it intercepts the outer wall of the net). (Figure by T. G. Leighton, S. D. Richards and P. R. White [2]).

It seems unlikely that humpback whales exploit sound for echolocation with bubble nets. Echolocation is normally associated with *odontoceti*, and although there are suggestions that humpbacks may echolocate [53,54], there is to date no evidence that they have used it to locate schools of prey. Although there is evidence of directionality in the songs of humpback whales [55,56], Figure 10(b) should not be interpreted as implying they can generate a 10° beam – we do not know one way or the other. Similarly, the highest reported frequencies generated by humpbacks correspond to harmonics in recordings in excess of 15 kHz [57] and 24 kHz [56], close to the bandwidth of the recording equipment. The following section will show that, if the bubble size distribution in cetacean bubble nets resembles that measured under ocean breaking waves, bubbles will increase the sound speed in the 30-50 kHz range (Figure 11(b)). Of course the ability to echolocate prey is well-known in *odontoceti*, although they can exploit frequencies so high that the sound

speed will probably tend to the bubble-free value (Figure 11(b)). At such frequencies and void fractions, the issue is less likely to be the effect of bubbles on the sound speed, and more their effect on attenuation. This will be the topic of the next section.

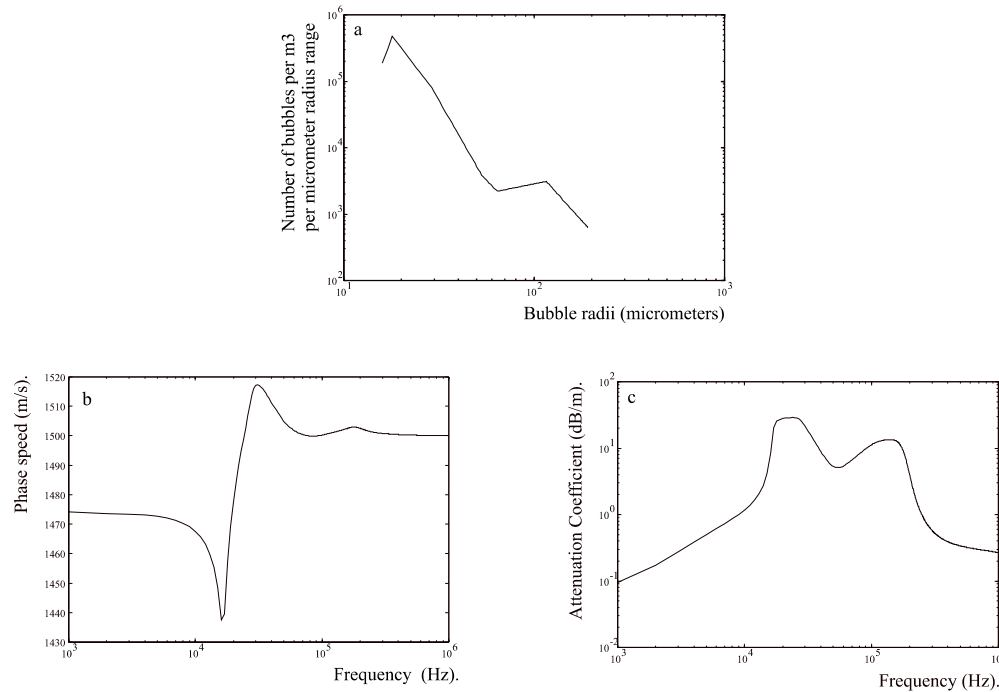


Figure 11. (a) The bubble population measured in the ocean in reference [58]. (b) The sound speed calculated for the bubble population of (a). (c) The attenuation calculated for the bubble population of (a). (Figure courtesy T. G. Leighton and S. D. Meers). See reference [1] for details.

3.2 Dolphin echolocation in bubbly water

The previous section discussed how some humpback whales may have found acoustics techniques for enhancing the performance of their bubble nets. They are not alone in using bubble nets to catch prey. Dolphins have also been observed to feed using bubbles [59] (Figure 12(a)-(d)). Indeed it is interesting to speculate that exploitation of the schooling of fish in response to startling via bubble acoustics is more widespread, if perhaps less elegant, than the scheme of Figure 12(b). The filming associated with Figure 12 [59] shows bubble plumes generated by gannets (Figure 12(e)-(g)) diving into a shoal of sardines which dolphins have herded to the sea surface. These plumes will no doubt complicate an underwater sound field already populated by the calls and bubble emissions of dolphins, and the entrainment noise of the gannet bubble plumes, and could further stimulate the sardines to school [60, 61, 62]. Gannets, dolphins, sharks and whales *etc.* (Figure 12(h)) all benefit from this, although to what extent this is intentional is unknown [60,61].

Odontoceti regularly exploit frequencies in excess of 100 kHz for echolocation. At such frequencies the bubble nets influence the sound field in a very different manner to that shown in Figure 10(b). First, at such high frequencies the bubbles could possibly increase the sound speed (making the net outwardly refracting, as shown in Figure 10(c)); whether this occurs would depend on the bubble size distribution, which is not known for bubble

nets. If however the net contained a size distribution typical for oceanic breaking waves, then at 100 kHz the sound speed would probably not be dissimilar from that of bubble-free water (note that in Figure 11(b) these wave-generated ocean bubbles increase the sound speed only in the range 30-50 kHz).

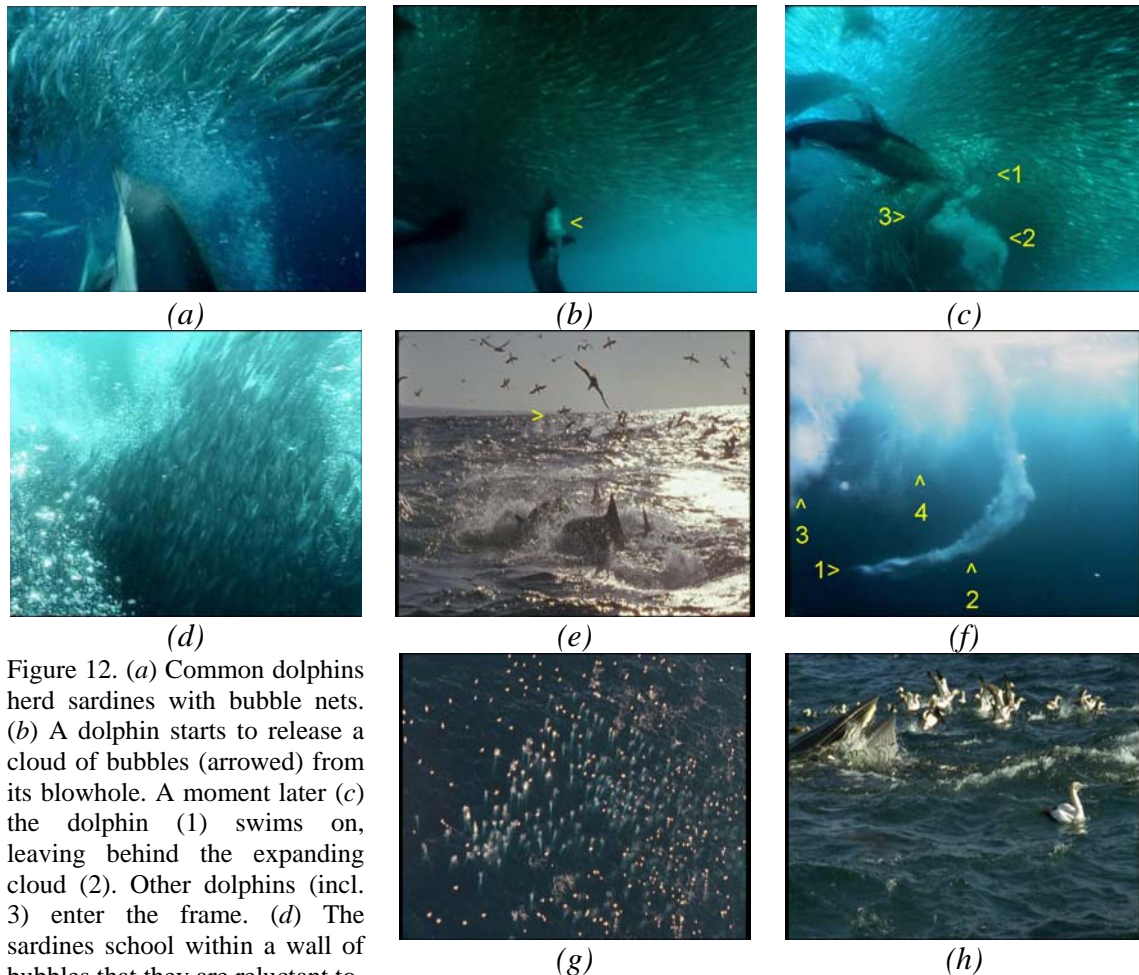


Figure 12. (a) Common dolphins herd sardines with bubble nets. (b) A dolphin starts to release a cloud of bubbles (arrowed) from its blowhole. A moment later (c) the dolphin (1) swims on, leaving behind the expanding cloud (2). Other dolphins (incl. 3) enter the frame. (d) The sardines school within a wall of bubbles that they are reluctant to cross, whilst (e) gannets dive into the sardine shoal to feed, folding their wings just before entry (arrowed). (f) On diving, a gannet (1) entrains a bubble plume (2). Plumes a few seconds old (3, with an older 4) have spread. (g) An aerial view shows hundreds of tight bubble plumes beneath airborne gannets. (h) A Bryde's Whale joins the feed. It surfaces with open mouth, which it then closes, sardines spilling from it. Images courtesy *The Blue Planet* (BBC). See also Byatt *et al.* [59].

Second, for the bubble population assumed in the plotting of Figure 10(b), the attenuation at 4 kHz (the higher end of the frequency range used in the feeding calls) has been calculated to be 6 dB/m. However at the higher frequencies used by dolphins in echolocation, the attenuation increases. At <100 kHz it is in excess of 200 dB/m.

This creates a dilemma. In creating bubble nets, either the dolphins are blinding their sonar when they need it most (i.e. when hunting in a visually complex environment); or they have sonar systems which out-perform the best man-made sonar. Given that dolphin sonar hardware has only mediocre properties compared to the best man-made sonar [46], if their

sonar is operational in bubble nets, it must be a result of the processing. Given the high amplitude pulses dolphins can generate, and the short ranges over which they are required to detect prey in bubble nets, it is not inconceivable that they are exploiting a nonlinearity. This will now be explored.

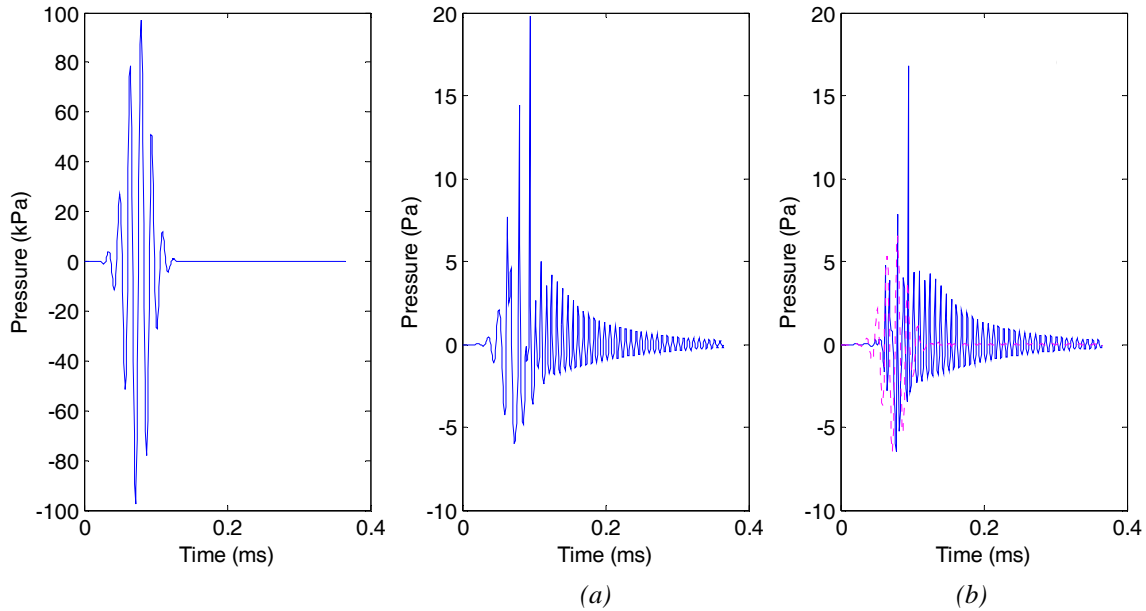


Figure 13. The driving pulse (centre frequency 65.7 kHz) used to insonify the systems of Figures 14-16

Figure 14. (a) Simulation of the pressure detected at a range of 1 m from a single monopole target used in Figure 15, and the bubble used in Figure 16, for insonification by the pulse shown in Figure 13. (b) The plot of Figure 15(a) is superimposed in red on the plot of Figure 14(a).

The above calculations indicated very high attenuations in bubbly water for frequencies associated with dolphin echolocation. However, as Leighton points out [61], such calculations assume that the bubbles undergo linear pulsations in the steady state, whereas dolphins use short pulses of sufficiently high amplitude to drive bubbles into nonlinear oscillation. A theory for modelling such acoustic propagation has recently been developed [22], together with an exploration of how these nonlinear effects might occur and indeed be exploited.

It is very likely that, for dolphin sonar to operate effectively in bubbly water, the dolphins must mentally be undertaking signal processing which takes into account the nonlinearities they are generating [61]. This is because, whilst the best manmade sonar hardware is superior to that available to dolphins [46], nevertheless the dolphins can echolocate in environments (bubbly water, sediments etc.) which confound the best man-made systems. The processing must therefore be making the difference. Given the severe scattering, attenuation and reverberation the dolphin must be counteracting, a nonlinear process would seem to be a strong possibility. Figures 13-16 illustrates one such route.

The pulse of Figure 13 is used to insonify a region of water containing both a linearly scattering target and an air bubble of radius 22.5 microns in water under 1 bar of static

pressure. All of the scattered waveforms in Figures 13-16 are simulated at a distance of 1 m from the target and bubble.

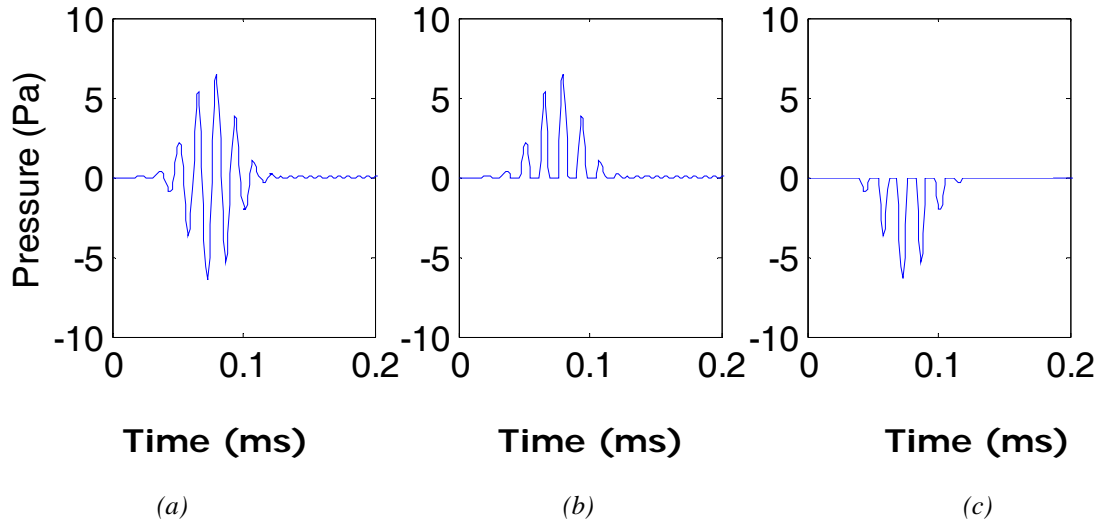


Figure 15. (a) The pressure signal from a single monopole linearly scattering target, simulated for measurement at a distance of 1 m from the target, for insonification by the pulse shown in Figure 13. (b) The positive half-wave rectification of the signal in (a). (c) The negative half-wave rectification of the signal in (a).

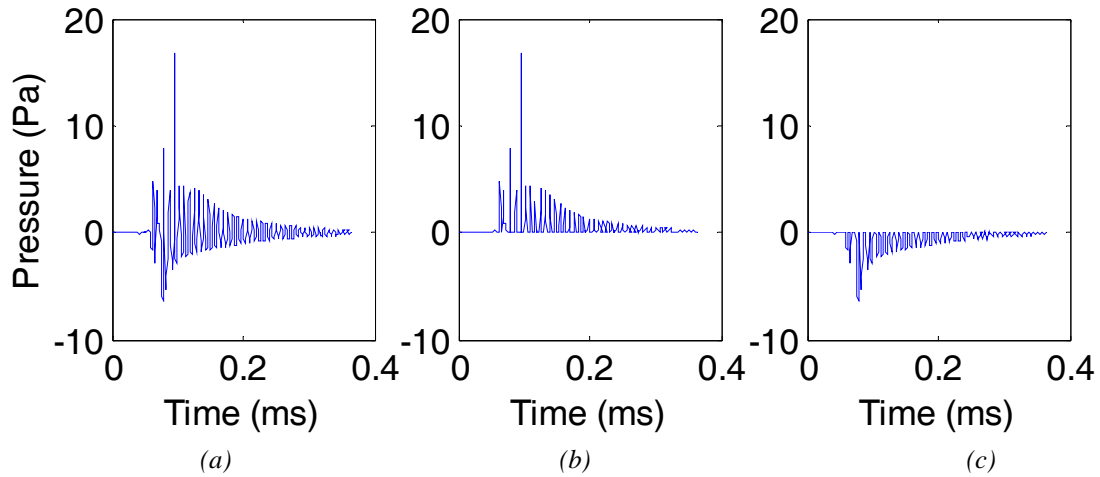


Figure 16. (a) The pressure signal scattered from a single air bubble of radius 22.5 microns in water, under 1 bar static pressure, simulated for measurement at a distance of 1 m from the target, for insonification by the pulse shown in Figure 13. Hence the air bubble is insonified at 67.5 kHz (a frequency which is close to the resonant frequency of the bubble). (b) The positive half-wave rectification of the signal in (a). (c) The negative half-wave rectification of the signal in (a).

Figure 14(a) shows the net scatter detected from the bubble and target. Whilst at first sight this may not seem to reveal much, when (in Figure 14(b)) the scatter from the target alone

(without the bubble, as calculated in Figure 15(a)) is superimposed on the signal in Figure 14(a), it is clear that the negative pressure component of the scattered signal more clearly shows the presence of the target than does the positive component. This is because the nonlinearity in the bubble response generates an asymmetry about the zero-pressure line, as will now be shown.

Parts (b) and (c) of Figure 15 show, respectively, the results when the signal in Figure 15(a) is subjected to positive and negative half wave rectification. The signal from the linearly scattering target contributes equally to both, such that the energy in Figures 15(b) and (c) are equal.

The nonlinearities in the scatter from the bubble create a different picture (Figure 16). The pressure scattered from the bubble is clearly asymmetrical about the zero-pressure axis. Parts (b) and (c) of Figure 16 show, respectively, the results when the signal in Figure 16(a) is subjected to positive and negative half wave rectification. The energy in Figure 16(b) is more the 2.1 times greater than that in Figure 16(c).

This asymmetry of course provides a method by which the signal from the linearly scattering target can be distinguished from the bubble, if both contribute to the scattered signal (Figure 14).

Hence when (in Figure 14(b)) the signal from the linearly scattering target (Figure 15(a)) is superimposed on the signal of Figure 14(a), the potential of the nonlinearity is clear: whilst the temporal peak energy in the scattered signal of Figure 14(b) comes from the bubble scatter, the temporal peak in the negative pressure comes from the linearly scattering target. Indeed Figure 15(b) illustrates how much of the early stages of the return in Figure 15(a) comes from the target. Of course, were the relative amplitudes of the scatter from target and bubble different, this simple result would not hold true, but the potential of the bubble nonlinearity to enhance the detection of targets and bubbles with respect to one another is clear.

Whilst illustrative, such examples should however be treated with care. There might, for example, be a temptation to quantify the enhancement in target detection by correlating the received signals with the driving pulse. However in Figures 14 and 16, the bubble is being driven close to half of its pulsation resonance frequency. The response from the bubble is almost entirely at the bubble resonance, whereas the response from the linear scatterer is at the frequency of the transmitted pulse. Hence it would be very easy to separate the linear from the non-linear responses, simply by filtering about the bandwidth of the transmitted pulse (which causes the bubble response to vanish almost completely). This is of course exactly what a correlation process does.

The correlation output, without or without rectification, would contain only the linear response. Hence a correlator would not help indicate any improvement obtained by rectification.

Indeed one might argue that you should look at the response at the output of a correlator, since this is the minimum that a standard sonar system would employ. At the output of

such a correlator you would not see an asymmetry in the waveform. This is because the correlator acts as a band-pass filter, with a fairly narrow pass band. To get asymmetry, the signal must have a spectrum that occupies more than an octave, which the output of a correlator will not, in general, achieve.

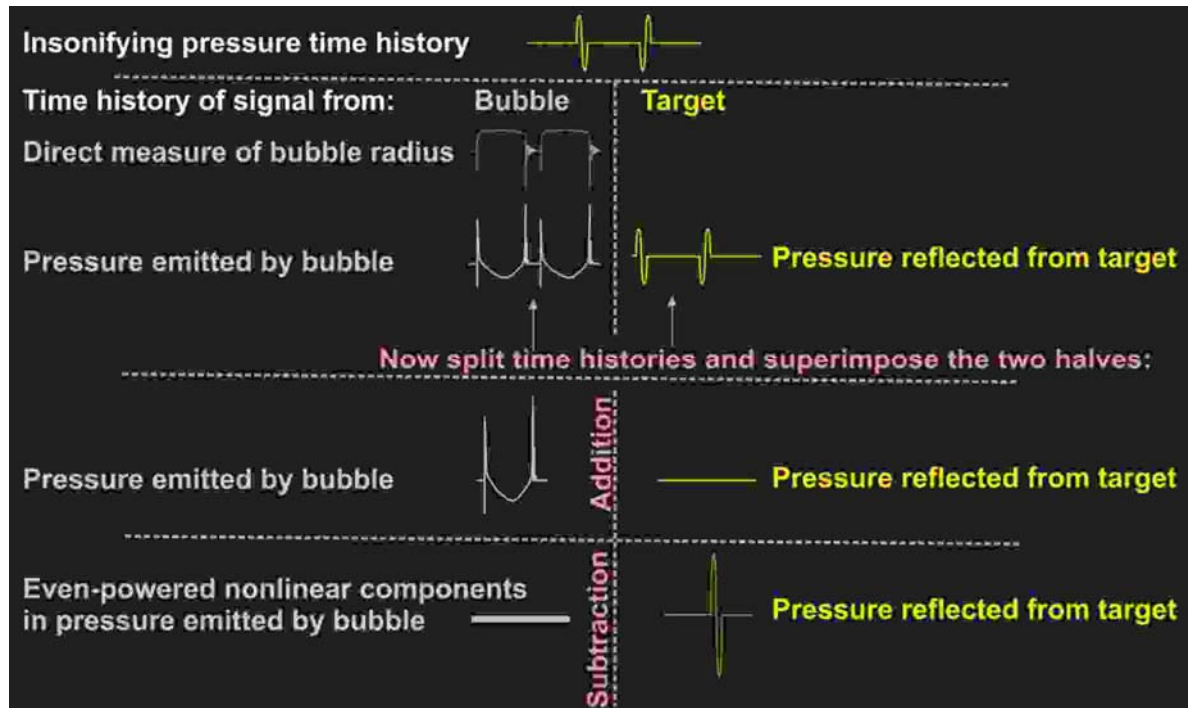


Figure 17. Schematic of a proposed 'Twin Inverted Pulse Sonar', whereby the scattering from a linear scatterer (such as a fish or a mine), and scattering from nonlinear scatterers (such as bubbles) can be enhanced and suppressed relative to one another. The linear signals (the driving sonar field and the scatter from the 'target') are shown in yellow; the even powered nonlinearities (from the bubble scatter) are shown in blue; and the processing instructions are shown in pink.

Another route for exploiting the nonlinearity to enhance target detection relies on the generation of even-powered terms in the expansion of the nonlinearity associated with the scatter from the bubble. Having identified a strong second harmonic [22], and noting that such even powered harmonics would be insensitive to the sign of the driving field, Leighton [22,61] suggested that the use of closely-spaced pulses of opposite polarity [60,61,62] illustrates just one of the ways in which the linear scatter from targets such as swim bladders driven off-resonance, or mines, might be enhanced compared to the scatter from oceanic bubble clouds. If the returned time series is split in half, then on subtraction of these two halves, the signal from the linearly scattering target doubles, whilst the energy invested in the even-powered harmonics of the scatter from the bubbles is suppressed (Figure 17). (Of course the linear and odd nonlinear terms will not be suppressed. This means that enhancement of the detection of linearly scattering targets compared to detection of bubbles in this way will not be as effective as the enhancement in the bubble scatter compared to that from linearly scattering targets which occurs when the two halves of the time series are added, as may be done with contrast agents).

Let us say the problem is to detect a linearly scattering target (the 'target') which is difficult to detect because it is immersed in a cloud of bubbly water. Such a target might be a fish in a dolphin bubble net - even with a swim bladder, the fish would produce ostensibly linear scatter from dolphin echolocation because the gas is driven so far from resonance. Alternatively, it might consist of a military mine which is a hazard to landing craft because it is hidden from sonar by breaking waves.

Consider if the emitted sonar signal were to consist of two high amplitude pulses, one having reverse polarity with respect to the other (Figure 17, top line). Linear reflection from the solid body is shown in Figure 17(b)(i). The bubble generates nonlinear radial excursions (Figure 17(a)(i)) and emits a corresponding pressure field (Figure 17(a)(ii)). Whilst the pressure emitted by the bubble may contain linear and odd-powered nonlinearities, it is the even powered (*e.g.* quadratic) nonlinearities which will be insensitive to the sign or the driving pulse, and hence which can be used to enhance the scatter from the target over that from the bubbles. It is these quadratic (and high even-powered components) which will be discussed in Figure 17, and below.

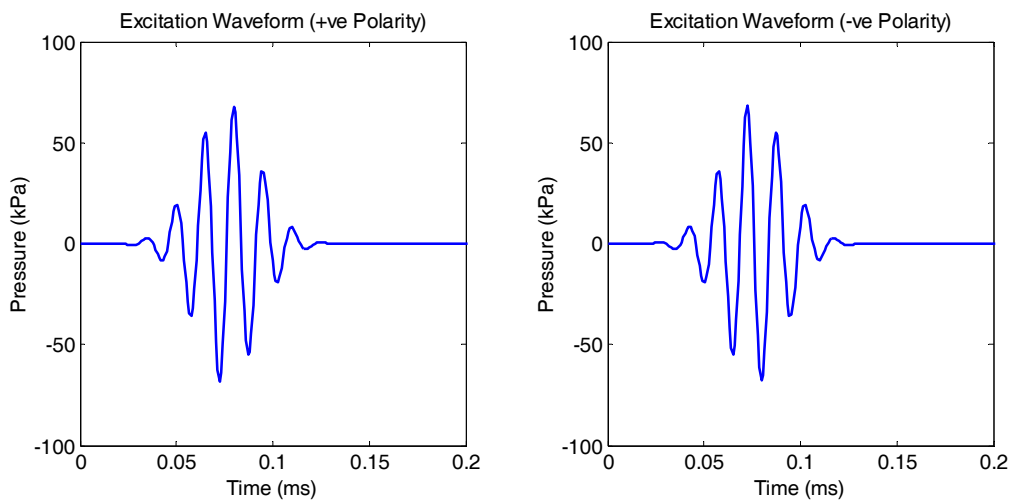


Figure 18. Two driving pulses which are used to insonify a bubble: one has negative polarity with respect to the other. The centre frequency of both pulses is 65.7 kHz

Normal sonar would not be able to detect the signal from the solid (Figure 17(b)(i)), as it is swamped by that from the bubbles (Figure 17(a)(ii)). If however the returned time histories are split in the middle and combined to make a time history half as long, enhancement and suppression occurs. If the two halves of the returned signals are added, the even-powered nonlinear components of the scattering from the bubble are enhanced (Figure 17(a)(iii)), whilst the signal from linearly scattering target is suppressed (Figure 17(b)(ii)). This can be used to enhance the scatter from biomedical contrast agents. If however the two halves of each returned signal are subtracted from one another, the even-powered nonlinear components of the scattering from the bubbles is suppressed (Figure 17(a)(iv)) whilst the reflections from the solid body are enhanced (with the usual constraints imposed by increased signal-to-noise ratio) (Figure 17(b)(iii)).

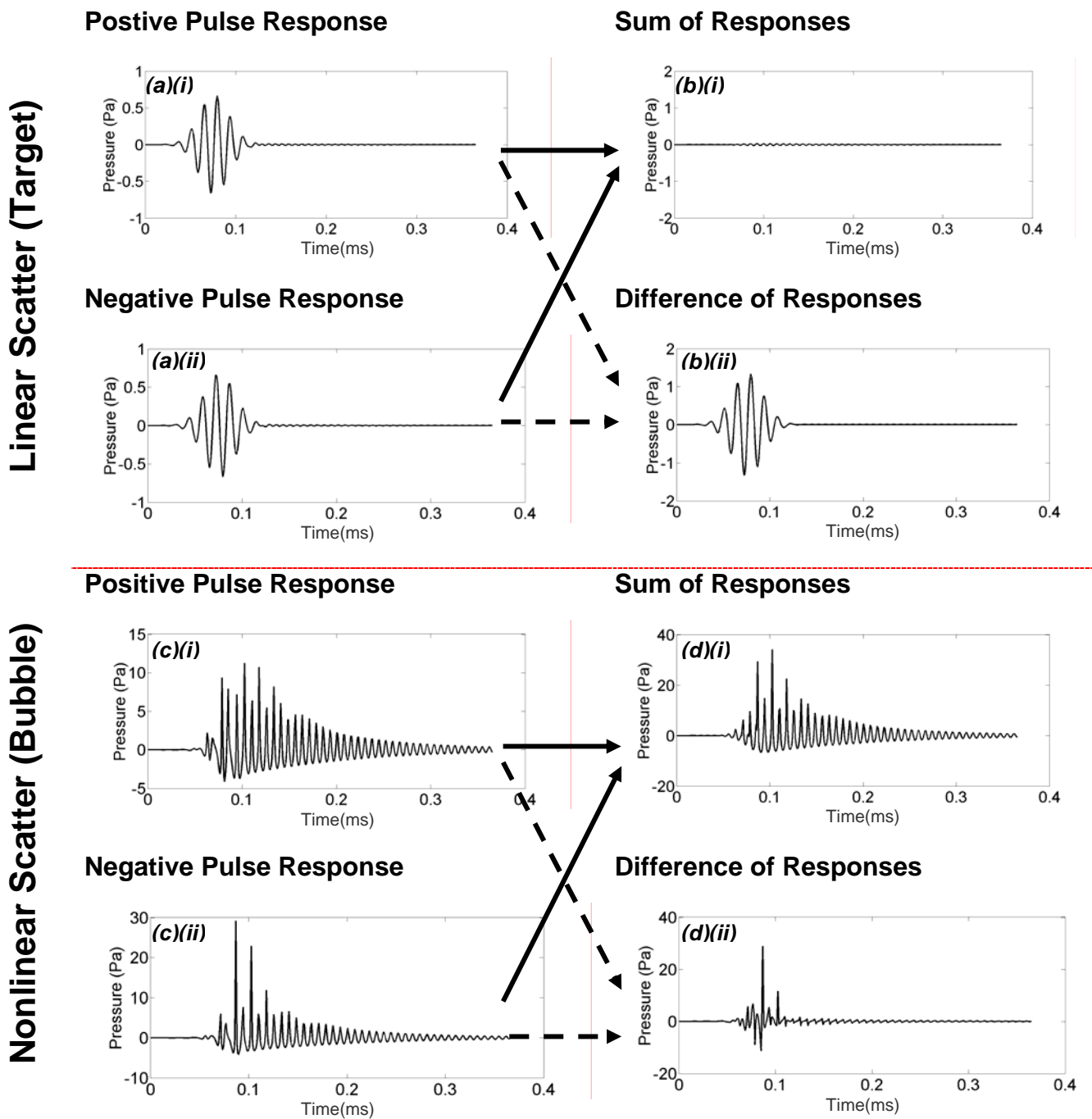


Fig. 19. The scatter that follows following insonification by the pulses from Fig. 18. The Fig. shows the linear scatter from the target (above the horizontal dashed red line, in (a) and (b)), and the scatter from a bubble (below the horizontal dashed red line, in (c) and (d)). The graph on the left in each case (i.e. (a) for the target; (c) for the bubble) shows the scatter from the pulses from Fig. 18: the upper plot (i) shows the scatter when excited by the ‘positive’ pulse of Fig. 18(a); the lower plot (ii) shows the scatter when excited by the ‘negative’ pulse of Fig. 18(b). The solid arrows indicate the process of addition, and the dashed grey arrows indicate the process of subtraction. The air bubble has radius 22.5 microns and is in water under a static pressure of 1 bar, insonified at its resonance frequency.

If echolocation is the equivalent of vision underwater, then switching from linear to nonlinear sonar in bubble clouds might find analogy with driving through fog. 'Linear headlamps' would provide the familiar backscatter from the fog, making detection of targets difficult (analogous to the intense sonar backscatter from bubbles). However switching to nonlinear sonar might be equivalent to turning on 'nonlinear headlamps' in a car, which backscatter far less from the fog and so make driving easier.

A preliminary calculation suggests that this technique may have the potential to enhance the detection of linearly scattering targets in bubble clouds. Figure 18 shows two driving pulses which are used to insonify a bubble: one has negative polarity with respect to the other. Figure 19 shows the linear scatter from the target (above the red line, in (a) and (b)), and the scatter from a bubble (below the red line, in (c) and (d)). The graph on the left in each case (i.e. (a) for the target; (c) for the bubble) shows the scatter from the pulses from Figure 18: the upper plot (i) shows the scatter when excited by the 'positive' pulse of Figure 18(a); the lower plot (ii) shows the scatter when excited by the 'negative' pulse of Figure 18(b).

The linear scatter of the positive pulse (Figure 19(a)(i)) is in antiphase with that from the negative pulse (Figure 19(a)(ii)), so that they add (the process indicated by the upper pair of solid arrows in Figure 19) they produce zero signal (the time history in Figure 19(b)(i) is not precisely zero because of numerical errors).

When they are subtracted from each other (the process indicated by the upper pair of dashed arrows in Figure 19), the amplitude of the signal is doubled, which is of course equivalent to a 6 dB increase over the energy in either of the original signals in (a).

However the nonlinear scatter by bubble of the positive pulse (Figure 19(c)(i)) is not in antiphase with that from the negative pulse (Figure 19(c)(ii)). Indeed, when they add (the process indicated by the lower pair of solid lines in Figure 19) they produce a signal (the time history in Figure 19(d)(i)) which is 5 dB greater than the average energy of the original signals in (c). When they are subtracted from each other (the process indicated by the lower pair of dashed arrows in Figure 19), the amplitude of the signal is 1 dB less than the average energy of the original signals in (c).

The key point to note here is that addition of signals in Figure 19 enhances the scatter of the bubbles compared to the linear scatter from the target; whilst subtraction does the opposite, enhancing the signal from the linearly scattering target compared to that of the bubbles. That it is easier to enhance the detection of bubbles compared to the linearly scattering target, than to do the converse, is of course expected, given that the bubble signal does not consist of purely even-powered nonlinearities.

Of course there are very many ways in which the nonlinearity generated by the bubbles may be exploited to enhance sonar detection of a linearly scattering target. If the receiver is narrowband, that proportion of energy which is at harmonics that are outside of its bandwidth will become 'invisible'. Even if the bandwidth of the receiver is sufficiently great to detect these harmonics, their higher frequencies may well be preferentially absorbed compared to the linear scatter from the fundamental (although an increase in

attenuation with frequency should not be taken for granted in bubble clouds, as it will tend to peak around the main resonance of the population – see Figure 20(c)).

The two examples shown above (asymmetry (Figures 14-16) and pulse inversion (Figures 18-19) have been demonstrated by using the scatter from a single bubble, and comparing it with a target which linearly scatters a similar amount of energy to that bubble.

Bubble populations at sea tend to have a wide size distribution (Figure 11(a)). One way of estimating the scatter and attenuation provided by a population of bubbles is through the use of acoustic scatter cross-sections. These have been used for several decades for predictions based on the assumption of linear bubble dynamics [63]. However recent developments in theory [22] have allowed the formulation of nonlinear acoustic cross-sections [64,65]. An example of their use will now be given.

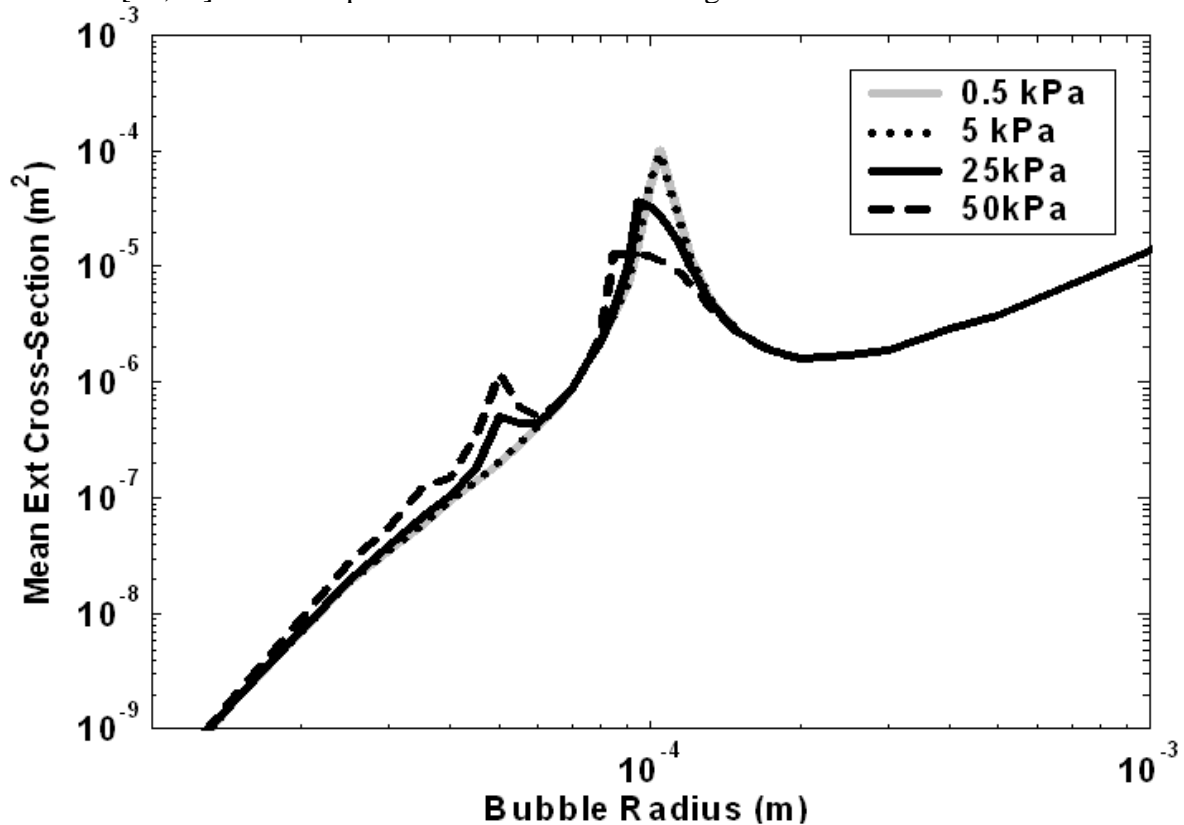


Figure 20. Acoustic extinction cross-section for a single bubble, as a function of the radius of that bubble, for insonification by a 1 ms duration pulse of 33 kHz centre frequency and 0-peak pulse amplitudes in the range 0.5-50 kPa. The cross-section calculated by the formulation of Leighton *et al.* [22] varies over time, and the figure plots its mean value. Although the 0.5 kPa and 5 kPa lines differ (particularly close to the fundamental resonance), they are barely distinguishable on this scale. Because the cross-section is not defined during ring-down [22], losses in that period cannot of course be included in this figure.

Source (see caption)	Value for x	Size range over which value for x holds (μm)	Measurement method	Environmental comments (location, windspeed etc.)
(i)	-6.4	35-50	Acoustic	3 m swell, 120 m water depth, 12 m/s wind, just outside Monterey bay. Hydrophone 25 cm below surface on average
	-2.2	60-280		
(ii)	-2.5	100-1000	Optical and acoustical	Wave height and period, respectively, 0.9 m and 7s. Wind speed between 3 and 5 m/s, west (247-258 deg). Water temp 18 deg c and beach slop 1.4 deg. Water depth 2 m. Surf zone, Scripps pier, La Jolla CA USA sea bed consists of fine, relatively uniformly grained lithogenous sand. Grain sizes from 0.2 to 0.5 mm diameter.
	-4.5	1000-5000		
(iii)	-2.0	37-150	Acoustical: Modulation frequency	Surf Zone, Tunstall, East Yorkshire (North Sea). 12-14 m/s wind speed
(iv)	-4.2	9-14	Acoustic inversion	Hurst Spit, Milford-on-Sea UK; gusts up to 50 mph.
(v)	-4.5	25-80	Nonlinear acoustic inversion	Hurst Spit, Milford-on-Sea UK; Mean wave height 1.0 m. Wind speed was SW at 4 m/s. Water temp at 8 deg C and air temp at 11 deg C. electrical conductivity was 49.5 mS/cm, pH was 8.07 and salinity 34.1%.
(vi)	-3.9	50-200	Photographic method	St Margaret's Bay, Nova Scotia Canada. Depth = 30 m. wind 8-10 ms, wave period 3.s wave height about 1.8 m. water temp 2 °C. Photographs taken at .7 m depth
(vii)	-4.1	17 – 63	Acoustical: Modulation frequency	50 cm below surface. Southampton UK; wind speed 10-12 m/s, gusting up to 16 ms. Depths of 17-22 m.
(viii)	-4.8	20 – 300	Multi-frequency inverted echosounder	0.1 m depth, FASINEX wind speed 12 m/s. 200 miles SW of Bermuda

Table 1. The values for x determined in a range of ocean measurements. Data taken from the following sources:

- (i) N Breitz and H Medwin, "Instrumentation for *in situ* acoustical measurements of bubble spectra under breaking waves" *Journal of the Acoustical Society of America*, **86** (2) August 1989, 739-743.
- (ii) G B Deane, "Sound generation and air entrainment by breaking waves in the surf zone" *Journal of the Acoustical Society of America*, **102** (5) November 1997, 2671-2689.
- (iii) A D Phelps, D G Ramble, T G Leighton, "The use of a combination frequency technique to measure the surf zone bubble population" *Journal of the Acoustical Society of America*, **101** (7) April 1997, 1981-1989.
- (iv) S D Meers, T G Leighton, J W L Clarke, G J Heald, H A Dumbrell, P R White, "The importance of bubble ring-up and pulse length in estimating the bubble distribution from acoustic propagation measurements" *Proceedings of the Institute of Acoustics: Acoustical Oceanography*, ed. T G Leighton, **23** (2) 2001, 233-241.
- (v) T G Leighton, S D Meers, and P R White, "Propagation through nonlinear time-dependent bubble clouds and the estimation of bubble populations from measured acoustic characteristics" *Proceedings of the Royal Society London A*, **460** 2004 2521-2550.
- (vi) B D Johnson and R C Cooke, "Bubble populations and spectra in coastal waters; A photographic approach," *Journal of Geophysical Research*, **84** (C7) 1979, 3791-3766.
- (vii) A D Phelps and T G Leighton, "Oceanic bubble population measurements using a buoy-deployed combination frequency technique" *IEEE Journal of Oceanic Engineering*, **23** (4) October 1998, 400-410.
- (viii) D M Farmer and S Vagle, "Waveguide propagation of ambient sound in the ocean-surface bubble layer" *Journal of the Acoustical Society of America*, **86** (5) November 1989, 1897-1908.

A not unexpected nonlinear effect in the steady-state would be a decrease in attenuation as the amplitude of the driving pulse increases (equivalent to a decrease in the acoustic absorption cross-section, with commensurate decrease in the acoustic scattering cross-section). This might be expected if the attenuation (and scatter) scale with the amplitude of

pulsation of the bubble. That is to say, we are assuming for the moment that, in the bubble population in question, it is the fundamental of the pulsation resonance (rather than, say, a geometrical affect) which is causing attenuation and scatter. As the driving amplitude increases, the amplitude of the bubble pulsation cannot increase proportionately: in the simplest illustration, the displacement on compression cannot of course be greater than the bubble radius. One source of this nonlinearity is the bubble stiffness [1]. Hence if the driving amplitude increases, the bubble response cannot increase proportionately, and we see a decrease in the ratio of the powers scattered and absorbed by the bubble, to the intensity of the incident driving field (the acoustic scatter and absorption cross-sections, respectively). This can be illustrated in Figure 20, where the peak corresponding to the bubble pulsation fundamental resonance decreases with increasing driving amplitude.

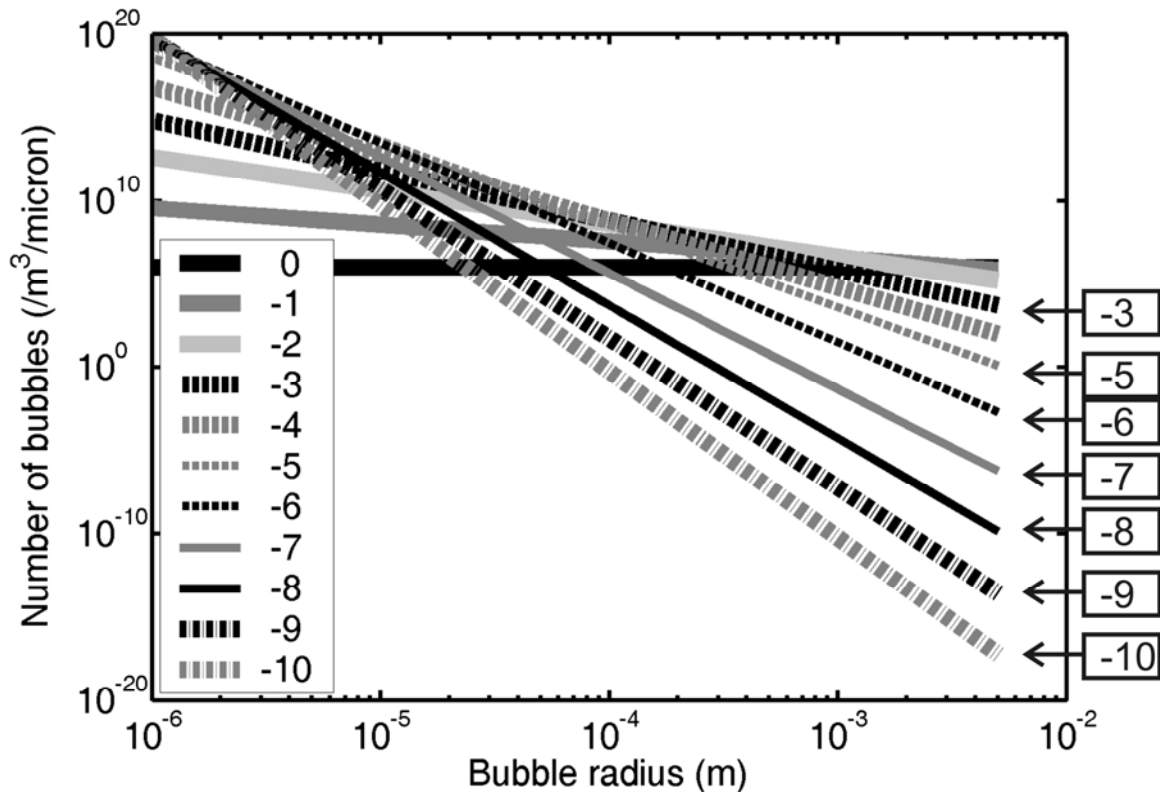


Figure 21. Various bubble populations, expressed in $n(R_0)$ (bubbles/m³ per micron bin width in radius) scaled such that the attenuation at low power levels in (b) will be the same for all bubble distributions.

However the picture is more complicated than the simple correspondence between fundamental resonance pulsation and attenuation/scatter assumed above. It is true that if the bubble population were to be dominated by resonant bubbles, the attenuation would decrease with driving amplitude. However with the decrease of the fundamental resonance peak in the acoustic extinction cross-section, there are corresponding increases in the cross-section corresponding to bubbles of particular radii. These are, specifically, about 50, 35 and 25 microns, equivalent to bubbles whose pulsation resonances would be multiples of the insonifying frequency (66, 99, 132 kHz respectively). If the bubble population were to be biased such that there were sufficient numbers of bubbles responding at the second harmonic, the growth in the peak would mean that attenuation could in fact increase with

driving amplitude. Figure 21 illustrates a range of bubble population distributions characterised by a power law, and Figure 22 plots the predicted attenuation as the amplitude of the driving field increases. For bubble populations with power law exponents between about -1 and -5, the general trend is that attenuation decreases with driving amplitude (as described above). This is a particularly fascinating prediction, given that many studies have measured such power laws in a variety of oceanic bubble populations, using a range of techniques (which of course can sample the population differently [2]). Specifically, Table 1 shows that values for x in the range -2 to -5 are not uncommon amongst at sea measurements.

However it is clear that for bubble populations with power law exponents of ~ -5.5 , increasing the driving amplitude can first decrease and then (at even higher drive amplitudes) increase the attenuation. Therefore by measuring the attenuation at various driving powers, it would for example be possible for a single-frequency source to gain information on the bubble size distribution over an octave or more.

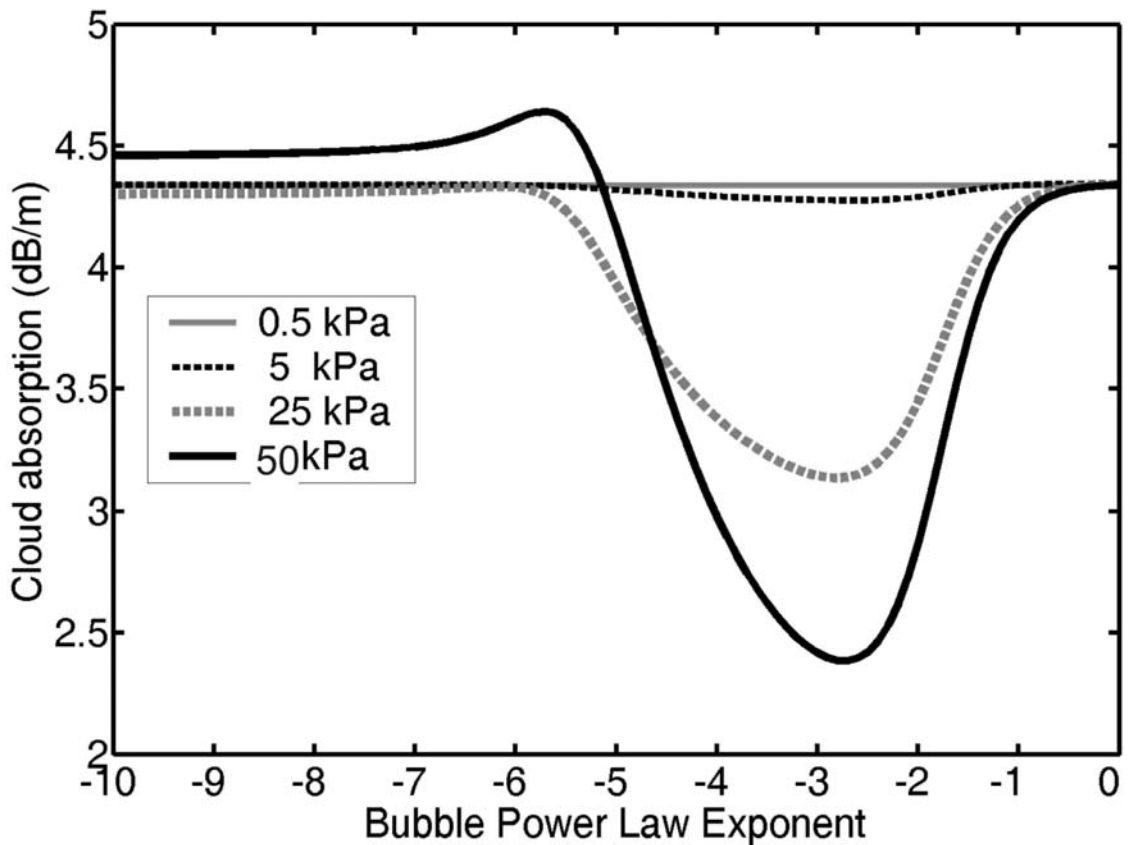


Figure 22. Cloud absorption for various power law bubble distributions $n(R_0) \propto (R_0)^x$ (for $x=0,-1,-2,\dots,-10$) where the number of bubbles is scaled as described in Figure 21, for insonification as in caption for Figure 20. Note that the constant offset at high power for -7 to -10 power laws might be due to rounding errors for the bubble response of a 1 micron bubble which is amplified by 10^{14} number of bubbles. The difference is not noticeable on the extinction cross-section plot.

4. CONCLUSIONS

This paper has outlined three possible applications of bubble acoustics in shallow water. The first relates to inversion of the entrainment sound generated by bubbles under waterfalls, breaking waves *etc.*, and was used to illustrate the potential applications of acoustics to space exploration. The other applications involved some of the interactions between the acoustic emissions of marine mammals, and the bubbly environment through which they may propagate. There is a wide range of techniques by which the nonlinearity in the scatter from a bubble may be used to enhance the detection of linearly scattering targets in oceanic bubble clouds.

Bubbles are ubiquitous in liquids in nature, and given their acoustical potency, the possible applications are fascinating.

REFERENCES

1. T.G. Leighton, *Bubble Acoustics from Seas to Surgeries*. Springer Series in Modern Acoustics and Signal Processing Series, Springer, 2005 (in preparation).
2. T.G. Leighton, From seas to surgeries, from babbling brooks to baby scans: The acoustics of gas bubbles in liquid, *International Journal of Modern Physics B*, **18**(25) 3267-3314 (2004).
3. A.D. Phelps and T.G. Leighton, The subharmonic oscillations and combination-frequency emissions from a resonant bubble: their properties and generation mechanisms, *Acta Acustica*, **83**, 59-66 (1997).
4. M.S. Longuet-Higgins Monopole emission of sound by asymmetric bubble oscillations, Part 1. Normal modes. *J. Fluid Mech.*, **201**, 525-541 (1989).
5. M.S. Longuet-Higgins, Monopole emission of sound by asymmetric bubble oscillations, Part 2. An initial value problem. *J. Fluid Mech.*, **201**, 543-565 (1989).
6. M.S. Longuet-Higgins, Resonance in nonlinear bubble oscillations, *J. Fluid Mech.*, **224**, 531-549, (1991).
7. M.S. Longuet-Higgins, Nonlinear damping of bubble oscillations by resonant interaction, *J. Acoust. Soc. Am.*, **91**, 1414-1422, (1992).
8. T.G. Leighton and A.J. Walton, An experimental study of the sound emitted from gas bubbles in a liquid, *European Journal of Physics*, **8**, 98-104, (1987).
9. M.R. Loewen and W.K. Melville, A model for the sound generated by breaking waves, *J. Acoust. Soc. Am.* **90**, 2075-2080, (1991).
10. J.A. Nystuen and M.J. McPhaden, The beginnings of operational marine weather observations using underwater ambient sound, In *Acoustical Oceanography, Proceedings of the Institute of Acoustics* Vol. **23** Part 2, T.G. Leighton, G.J. Heald, H. Griffiths and G. Griffiths, (eds.), Institute of Acoustics, 135-141 (2001).
11. T.G. Leighton, M.F. Schneider and P.R. White, Study of bubble fragmentation using optical and acoustic techniques, *Sea Surface Sound 94. Proceedings of the 3rd Meeting on Natural Physical Processes related to Sea Surface Sound*, M.J. Buckingham, J.R. Potter, eds., (World Scientific Publishing Ltd., Singapore) 414-428, (1995).
12. R. His, M. Tay, D. Bukur and G. Tatterson, Sound spectra of gas dispersion in an agitated tank, *The Chemical Engineering Journal*, **31**, 153-161 (1985).
13. L.S. De More, W.F. Pafford and G.B. Tatterson, Cavity sound resonance and mass transfer in aertated agitated tanks, *AIChE Journal*, **34**, 1922-1926 (1988).
14. J.W.R. Boyd and J. Varley, Sound measurement as a means of gas-bubble sizing in aerated agitated tanks, *AIChE Journal*, **44**, 1731-1739 (1998).
15. A.B. Pandit, J. Varley, R.B. Thorpe and J.F. Davidson, Measurement of bubble size distribution: An acoustic technique, *Chemical Engineering Science*, **47**, 1079-1089 (1992).

-
16. R. Manasseh, R.F. LaFontaine, J. Davy, I. Shepherd and Y.G. Zhu, Passive acoustic bubble sizing in sparged systems, *Experiments in Fluids*, **30** (6), 672-682 (2001).
 17. T.A. Sutter, G.L. Morrison and G.B. Tatterson, Sound spectra in an aerated agitated tank, *AIChE Journal*, **33**, 668-671 (1987).
 18. W.R. Usry, G.L. Morrison and G.B. Tatterson, On the interrelationship between mass transfer and sound spectra in an aerated agitated tank, *Chemical Engineering Science*, **42**, 1856-1859 (1987).
 19. T.G. Leighton, K.J. Fagan and J.E. Field, Acoustic and photographic studies of injected bubbles, *European Journal of Physics*, **12**, 77-85, (1991).
 20. T.G. Leighton, P.R. White and M.F. Schneider, The detection and dimension of bubble entrainment and comminution, *J. Acoust. Soc. Am.*, **103**, 1825-1835 (1998).
 21. <http://www.isvr.soton.ac.uk/fdag/Cross-faculty%20UUA%20centre/Acoustical%20Oceanography%201.HTM>
 22. T.G. Leighton, S.D. Meers and P.R. White, Propagation through nonlinear time-dependent bubble clouds, and the estimation of bubble populations from measured acoustic characteristics. *Proceedings of the Royal Society A*, **460**(2049) 2521-2550, 2004.
 23. L.L. Foldy, The multiple scattering of waves, *Phys. Rev.*, **67**, 107-119 (1945).
 24. S.G. Kargl, Effective medium approach to linear acoustics in bubbly liquids. *J. Acoust. Soc. Am.*, **111**, 168-173 (2002).
 25. A. Prosperetti, Bubble-related ambient noise in the ocean, *J. Acoust. Soc. Am.*, **78**, S2 (1985)
 26. W.M. Carey, Low-frequency ocean surface noise sources. *J. Acoust. Soc. Am.*, **78**, S1-S2 (1985)
 27. T.G. Leighton, P.R. White P.R. C.L. Morfey, J.W.L. Clarke, G.J. Heald, H.A. Dumbrell and K.R. Holland, The effect of reverberation on the damping of bubbles, *J. Acoust. Soc. Am.*, **112**(4), 1366-1376 (2002).
 28. D.L. Miller, On the oscillation mode of gas-filled micropores. *J. Acoust. Soc. Am.* **77**, 946-953 (1985).
 29. R.M. Quain, R.C. Waag and M.W. Miller, The use of frequency mixing to distinguish size distributions of gas-filled micropores. *Ultrasound Med. Biol.*, **17**, 71-79 (1991).
 30. H.N. Oguz and A. Prosperetti, The natural frequency of oscillation of gas bubbles in tubes. *J. Acoust. Soc. Am.*, **103**, 3301-3308 (1998).
 31. X. Geng, H. Yuan and A. Prosperetti, The oscillations of gas bubbles in tubes: Experimental results. *J. Acoust. Soc. Am.*, **106**, 674-681 (1999).
 32. T.G. Leighton, P.R. White and M.A. Marsden, The one-dimensional bubble: An unusual oscillator, with applications to human bioeffects of underwater sound, *European Journal of Physics*, **16**, 275-281, (1995).
 33. T.G. Leighton, P.R. White and M.A. Marsden, Applications of one-dimensional bubbles to lithotripsy, and to diver response to low frequency sound, *Acta Acustica*, **3**, 517-529, (1995).
 34. T.G. Leighton, D.G. Ramble, A.D. Phelps, C.L. Morfey and P.P. Harris, Acoustic detection of gas bubbles in a pipe, *Acta Acustica*, **84**, 801-814 (1998).
 35. T.G. Leighton, W.L. Ho and R. Flaxman, Sonoluminescence from the unstable collapse of a conical bubble, *Ultrasonics*, **35**, 399-405 (1997).
 36. T.G. Leighton, A.D. Phelps, B.T. Cox and W.L. Ho, Theory and preliminary measurements of the Rayleigh-like collapse of a conical bubble, *Acta Acustica*, **84**, 1014-1024, (1998).
 37. T.G. Leighton, B.T. Cox and A.D. Phelps, The Rayleigh-like collapse of a conical bubble, *J. Acoust. Soc. Am.*, **107**, 130-142 (2000).
 38. T.G. Leighton, B.T. Cox, P.R. Birkin and T. Bayliss, The Rayleigh-like collapse of a conical bubble: Measurements of meniscus, liquid pressure, and electrochemistry, *Proceedings of the 137th Regular Meeting of the Acoustical Society of America and the 2nd Convention of the European Acoustics Association (Forum Acusticum 99, integrating the 25th German Acoustics DAGA Conference)*, Paper 3APAB_1 (March 1999).
 39. Q.D. Chen, L.M. Fu, X.C. Ai, J.P. Zhang and L. Wang, Ultrabright cavitation luminescence generation and its time-resolved spectroscopic characterisation, *Physical Review E*, **70**(4 Pt. 2), 047301 (2004)
 40. D.D. Symons, Inertial liquid loading on the nozzle of a needle-free injection system, *Proc. Instm. Mech. Engrs.*, **218**, 233-240 (2004).
 41. M. Minnaert, On musical air-bubbles and sounds of running water, *Phil. Mag.*, **16**: 235-248 (1933).

-
42. T.G. Leighton and P.R. White, The sound of Titan: a role for acoustics in space exploration, *Acoustics Bulletin* **29**, 16-23 (2004).
43. T.G. Leighton, The Inaugural Medwin Award Address – Surf zone bubble spectrometry: The role of the acoustic cross section, *J. Acoust. Soc. Am.*, **110**(5) Part 2, 2694, (2001).
44. S. Thorpe, On the clouds of bubbles formed by breaking wind-waves in deep water, and their role in air-sea gas transfer. *Philos. Trans. R Soc London, A* **304**, 155-210 (1982)
45. M.S. Longuet-Higgins, 'The crushing of air cavities in a liquid,' *Proc. R. Soc. London*, **439**, 611–626 (1992).
46. W.W.L. Au, The Dolphin Sonar: Excellent capabilities in spite of some mediocre properties, Eds. M. B. Porter, M. Siderius and W. Kuperman, American Institute of Physics, Melville, New York (in press) (2004).
47. T.G. Leighton, S.D. Richards and P.R. White, Trapped within a wall of sound: A possible mechanism for the bubble nets of humpback whales, *Acoustics Bulletin* 2004; 29: 24-29.
48. F.A. Sharpe and L.M. Dill, The behaviour of Pacific herring schools in response to artificial humpback whale bubbles. *Canadian Journal of Zoology-Revue Canadienne de Zoologie* 1997; 75: 725-730.
49. T. Akamatsu, A. Nanami and H.Y. Yan, Spotted sardine *Sardinops melanosticus* listens to 1 kHz sound by using its gas bladder, *Fisheries Science* 2003; 69: 348-354.
50. Jensen FB, Kuperman WA, Porter MB and Schmidt H. *Computational Ocean Acoustics*, New York: Springer-Verlag, 2000.
51. T.G. Leighton, *The Acoustic Bubble*. London: Academic Press, 1994, pp. 58-59, 288-301, 302-308.
52. H. Williams. *Whale Nation*, London: Jonathan Cape (now part of Random House) (1988).
53. L.N. Frazer and E. Mercado, A sonar model for humpback whale song *IEEE J. Oceanic Engineering* 2000; **25** (1): 160-182.
54. E. Mercado and L.N. Frazer, *IEEE J. Oceanic Engineering*, **26**(3): 406-415 (2001).
55. C. Levenson. Characteristics of sound produced by humpback whales (*Megaptera novaeangliae*) in *NAVOCEANO Technical Note 7700-6-72*, Washington, DC: Naval Oceanographic Office, 1972.
56. W.W.L. Au, A.A. Pack, M.O. Lammers, L. Herman, K. Andrews and M. Deakos, The acoustic field of singing humpback whales in the vertical plane, *J. Acoust. Soc. Am.*, **113**: 2277 (2003).
57. W.W.L. Au, D. James and K.J. Andrews, *J. Acoust. Soc. Am.*, 110: 2770 (2001).
58. A.D. Phelps and T.G. Leighton, Oceanic bubble population measurements using a buoy-deployed combination frequency technique, *IEEE Journal of Oceanic Engineering*, **23**(4), 400-410 (1998).
59. A. Byatt, A. Fothergill, M. Holmes and Sir David Attenborough. *The Blue Planet*, BBC Consumer Publishing (2001).
60. T.G. Leighton. Nonlinear Bubble Dynamics And The Effects On Propagation Through Near-Surface Bubble Layers, *High-Frequency Ocean Acoustics*, Eds. M.B. Porter, M. Siderius and W. Kuperman, American Institute of Physics, Melville, New York (in press) (2004).
61. T.G. Leighton (2004), <http://www.isvr.soton.ac.uk/fdag/UAUA/research.html>
62. T.G. Leighton, The 2001 Tyndall Medal Address -- From sea to surgeries, from babbling brooks to baby scans: Bubble acoustics at ISVR, *Proceedings of the Institute of Acoustics*, Vol. **26** Part 2 (2004).
63. H. Medwin and C.S. Clay, *Fundamentals of Acoustical Oceanography*, (Academic Press) (1998).
64. T.G. Leighton and H.A. Dumbrell. New approaches to contrast agent modelling, *Proceedings of the First Conference in Advanced Metrology for Ultrasound in Medicine, Journal of Physics: Conference Series* **1**, 91-96 (2004).
65. T.G. Leighton, H.A. Dumbrell, G.J. Heald and P.R. White, The possibility and exploitation of nonlinear effects in the near-surface oceanic bubble layer, *Proceedings of the Seventh European Conference on Underwater Acoustics* 205-210 (2004).